Soft Matter

Transient stress and fabric model for quasi-static granular flows in three dimensions

Journal:	*Soft Matter*
Manuscript ID	SM-ART-12-2024-001535.R1
Article Type:	Paper
Date Submitted by the Author:	16-Feb-2025
Complete List of Authors:	Rojas Parra, Eduardo Andrés; University of Antofagasta, Department of Mechanical Engineering Kamrin, Ken; UC Berkeley, Mechanical Engineering

Soft Matter

ARTICLE TYPE

Cite this: DOI: 00.0000/xxxxxxxxxx

Transient stress and fabric model for quasi-static granular flows in three dimensions

Eduardo Rojas,[a] and Ken Kamrin [b]

Received Date
Accepted Date

DOI: 00.0000/xxxxxxxxxx

We present and validate a general three-dimensional continuum model for predicting the coupled fabric and stress transient response in 3D dense granular flows for the quasi-static regime. The model is inspired by isotropic and kinematic hardening theory widely applied to plastic loading cycles in metals, which constitutes a connection between two different flowing materials through the same plastic modeling framework. The first part of the model consists of a differential evolution equation for the fabric tensor, which incorporates a new parameter called *contact persistence* to model the capacity of the fabric network to keep its contacts according to the relative direction of the shear-rate. The second part of the model is an expression for the shear stress comprised of a backstress, proportional to the fabric tensor, and a term proportional to the shear-rate direction. This shear stress decomposition was obtained from DEM data extracted within a 3D Couette cell during unsteady processes wherein the shear-rate direction rotates instantaneously with respect to the axis perpendicular to the walls of the cell. The results of the model are compared with DEM simulations for different changes in shear orientation, achieving a good agreement for the evolution of the fabric and deviatoric stress tensors. The model is shown to be compatible with the second law of thermodynamics, revealing that the origin of the backstress flow resistance in granular media is distinct from the cause of backstresses in metals; rather than arising from stored defect energy, it arises from the dependence of dilatancy on the alignment of the fabric and flow-rate.

1 Introduction

Flowing granular materials are commonly found in geophysical and industrial processes as well as in our everyday life. The granular flow produced between tectonic plates during an earthquake, the flow of grain in a silo, and dry rice pouring from a bowl to a pot, are just a few examples of an enormous variety of processes where particles move as a granular assembly. These flows present a more diverse phenomenology than Newtonian viscous liquid flows because of a complex interplay between three different scales. The first scale corresponds to the microscale, associated with the dynamics of individual grains, the second is the mesoscale related to the connection between grains forming force chains, and the last corresponds to the macroscale determined by the size of the flowing region. An important connection between two of these scales was made through the dimensionless variable called *inertial number*: $I = d\dot{\gamma}/\sqrt{p/\rho_p}$,[1–4] where d corresponds to the mean diameter of particles, $\dot{\gamma}$ represents the shear-rate, p the confining pressure, and ρ_p the density of grains' material. This inertial number, obtained specifically for hard particles subjected to steady simple shear, can be interpreted as a ratio of microscopic to macroscopic time scales $I = t_{mic}/t_{mac}$, where $t_{mic} = d/\sqrt{p/\rho_p}$ represents the time that a particle spends entering a hole of diameter d under the unbalanced action of the pressure.[1] The macroscopic time $t_{mac} = 1/\dot{\gamma}$ is related to the global movement of the medium. The inertial number is formed by all the input variables involved in simple shear and I is the only dimensionless control variable in a system of quasi-monodisperse hard particles.[1] Accordingly, outputs like the effective friction coefficient defined as the ratio between shear stress and pressure $\mu = \tau/p$, depend only function of I, which gives us the inertial rheology: $\mu = \mu(I)$.

The inertial rheology can be written in a tensorial form for flows where the velocity field $\mathbf{v}$ is not one-dimensional, assuming that the shear-rate tensor $\mathbf{D} = \frac{1}{2}\left(\nabla\mathbf{v} + (\nabla\mathbf{v})^T\right)$ and shear stress tensor are aligned,[5,6] that is:

$$\boldsymbol{\tau} = \frac{\mu(I)p}{\sqrt{2}}\frac{\mathbf{D}}{|\mathbf{D}|}. \tag{1}$$

Here, $\boldsymbol{\tau} = \boldsymbol{\sigma}' \equiv \boldsymbol{\sigma} - (\mathrm{tr}\,\boldsymbol{\sigma})\mathbf{I}/3$ is the stress deviator, the modulus for tensors is defined as: $|\mathbf{M}| = \sqrt{\sum_{i,j} M_{ij}M_{ij}}$. This 3D model considers the granular medium as an incompressible fluid to impose the condition $\mathbf{D} = \mathbf{D}'$.[4]

The $\mu(I)$ rheology and its 3D extension have some impor-

[a] Department of Mechanical Engineering, University of Antofagasta, Antofagasta, Chile. E-mail: eduardo.rojas@uantof.cl
[b] Department of Mechanical Engineering, University of California, Berkeley, USA. E-mail: kkamrin@berkeley.edu

tant limitations. In general, the inertial rheology has important discrepancies with experiments and DEM simulations in non-homogeneous fields.[7,8] In these cases non-local effects associated with a cooperative behaviour of the granular medium emerge. The cooperative behaviour or non-local effect has been modeled principally based on second-order partial differential equations as in the *granular fluidity model*,[9–11] and in the *μ-corrected model*.[12,13]

Up to this point, we have only consider steady granular flows, condition where the inertial rheology and its non-local corrections were obtained. These steady models have been formulated without explicitly considering the mesoscale, intimately linked to transient processes. The mesoscale in dense granular flows takes the form of *force networks*, commonly called *force chains*, a concept reinforced during the 70's decade by the intensive use of new photo-elastic techniques and discrete element methods.[14,15] Transient shear-rate inputs have an important effect on forces chains which has been studied in Utter *et al.*[16] Essentially, when a flowing granular material at steady state experiences a rapid change in the shear-rate direction (or magnitude), a change in the force chains follows but is not instantaneous, because there is a finite relaxation time needed for the rearrangement of the contact network.[17] The contact network, and thus the system's stress, is strongly linked to the force chains and represents a physical structure of granular assemblies that strengthens them. Several forms have been developed to capture the evolving strength response through transient models, but due to the complexity of the problem, a variety of frameworks with different level of detail have been presented. In general, some transient cases can be treated in a simplified way, especially when the shear-rate does not change its direction drastically. On the other hand, the presence of large changes in the share-rate direction (for example a shear-rate reversal), requires more sophisticated models. A simple categorization for transient models is given below.

Steady state approximation: Well-known relations for steady flows, like the inertial rheology have been applied to solve transient granular flows in processes where the contact network does not change its direction dramatically. One example corresponds to the collapse of a granular column, where particles fall down rapidly and form a heap. Here, many authors have used constitutive steady-state models to estimate the surface profiles of the granular medium, obtaining a good agreement with experiments and DEM simulations. In Lacaze *et al.*[18] the inertial rheology $\mu = \mu(I)$ was verified in data collected from discrete element simulations during the collapse of a cylindrical column of granular matter. Then, this case was simulated as a continuum medium by using the local inertial rheology[19–23] and later by adding a non-local relation as in Lin *et al.*[24]. Another configuration where steady-state relations are used to approximate transient flows corresponds to granular avalanches on smooth surfaces. In Juez *et al.*[25] the depth-averaged procedure, along with some empirical shear stress relations is performed to simulate a mass of particles falling down by gravity on a curved floor, while in Gray *et al.*[26] the Mohr-Coulomb yield criterion is used in a similar configuration. Note that the depth-averaged method is applicable if the movement of the fluid has predominantly one direction of flow, which is also a condition for minimizing structural changes in granular media. A similar depth-averaged approach based on steady-state rheology was used earlier to predict the formation of Kapitza waves on the surface of inclined granular beds, which are unsteady features[27].

Plasticity without an explicit anisotropic variable: Plasticity theory and its variants can be used for modeling transient granular flows without including explicitly a new variable to represent the structural anisotropy of the medium. This framework has been mainly restricted to model dry sand and soils at small and large scale. One of these frameworks is the visco-elasto-plastic model proposed by Babeyco *et al.*[28] for simulating the transient subducting movement of tectonic plates. The zone of fluidization between plates is assumed to be a Maxwell visco-elastic material. Several continuum granular simulations of plasticity theory combine with the critical state concept to couple strength and dilatancy.[29] For example, in Khalili *et al.*[30] a model based on the plastic-bounding-surface theory plus a modified critical state line is used to mirror complex strain-stress cycles for drained sand. More model combinations involving critical state theory include Golchin *et al.*,[31] where a hyper-elasticity model is presented to simulate loading and unloading in triaxial tests for sand; and Yin *et al.*[32], where a double-yield-surface framework is developed for clay. Other plasticity frameworks applied to transient problems include hypo-plasticity[33] and visco-plasticity.[34]

Anisotropic models: In granular matter there exists an anisotropy associated to the particles' shape and another to the contact distribution among the particles. In this paper we only consider contact anisotropy, which can be isolated by keeping particle shapes spherical. To model the anisotropy, a homogenized state variable must be evolved according to a differential equation. Most continuum models focus essentially on quasi-static processes occurring for $I < 10^{-3}$,[2,35] and they can be split into three types:

1. Scalar anisotropy: Like stresses and deformations, the contact structure of a granular medium has major and minor directions, which indicates a tensorial representation. In some cases the anisotropy can be reduced to a scalar variable, as in the model presented in Magnanimo *et al.*[36] This model is formed by two scalar differential equations to replicate results obtained from DEM simulations. The first equation is for the stress, and the second is an evolution equation for a scalar structural anisotropy. A more general version of this model is shown in Kumar *et al.*[37]

2. Fabric tensor evolution equation: A more direct way to represent the anisotropy is by forming a tensor from the contact directions between grains. The evolution of this *fabric* tensor is governed by a differential equation[38,39] that must obey certain representation theorems[40] arising from the objectivity principle. These requirements constrain how to express the fabric evolution equation in terms of the other tensors

involved, but still ultimately some coefficients have to be fitted.[41] Fabric evolution models of this type have also been used to model anisotropy of particle orientations for aspherical grains.[42]

3. Backstress evolution equation: A *backstress* is a tensorial, stress-united state variable commonly used in fields like metal plasticity to model evolving, direction-dependent shear strength. The shear resistance in models of this type, known collectively as *kinematic hardening* models, is the sum of a backstress and an isotropic resistance to plastic deformation. The concept has been extended to transient strength in granular media; for example, Nemat-Nasser *et al.*[43] proposed a kinematic hardening model that considers a backstress proportional to the fabric tensor. Thus, backstress models for granular media can be a *type* of fabric model.

Below, a new stress and fabric model for dense granular flows during transient 3D shearing is presented. The model is based on isotropic and kinematic hardening theory. Specifically, the model considers the deviatoric stress tensor as the sum of a backstress proportional to the fabric tensor, plus an isotropic part proportional to the unit shear-rate tensor. A tensorial differential evolution equation for the fabric is also proposed. This equation includes a key new parameter called *contact persistence* to consider the capacity of a granular assembly to maintain its contacts depending on the shear-rate direction with respect to the fabric. Three-dimensional DEM simulations were performed in a Couette cell, where the shear-rate tensor was rotated through various angles with respect to the axis perpendicular to the cell walls. The objective of this rotation is to produce an evolution of the fabric and stress out of the plane of the shear deformation, which is not possible in previous 2D configurations.[38,39,43]These kind of protocols to produce transients have also been used in other related areas like suspensions.[44–46] Lastly, we will analyze the newly proposed model thermodynamically and show how, when coupled to a proper dilatancy relation, the model necessarily satisfies the second-law requirement of non-negative dissipation.

2 Numerical setup

The setup consists of a 3D planar Couette cell formed by a granular medium of spherical particles confined between two rough square walls (see Fig. 1). Periodic boundary conditions are applied to all lateral sides of the cell. To avoid segregation or crystallization, the diameters of the internal spheres follow a uniform distribution in the range $[0.5d, 1.5d]$, where d is the average diameter. The mass density of particles ρ_p is constant. The walls are made of spheres of diameter d, and they are two layers thick. The first layer is a compacted square-planar configuration, and the second layer is made of spheres alternating with empty spaces to increment the walls' roughness. The width of the cell is $W = 20d$ and the height between walls is $H = 17d$.

The numerical setup is built on the DEM platform Yade.[47] The sphere interactions are simulated with frictional-visco-elastic forces in the normal and tangential directions. The normal rigidity k_n of the particles is set to produce a characteristic mean overlap of $\delta = pd^2/k_n = 0.0005d$, ensuring that the medium remains in the quasi-rigid regime. The tangential rigidity is $k_t = 0.5k_n$.[17] The normal and tangential damping constants c_n and c_t are fixed to achieve a restitution coefficient equal to 0.5. A tangential Coulomb friction is added with a friction angle equal to 24°.

The vertical movement of the walls (parallel to $\hat{\mathbf{e}}_2$) is controlled by a proportional control system as in Rojas *et al.*[39] to produce a constant normal stress p in the granular medium. The walls are also subjected to a periodic horizontal velocity $\vec{U}_w$ to produce a transient shear-rate. The period T is divided into two parts. During the first part, from $t = 0$ to $t = T/2$, the velocity of the top wall is in the $\hat{\mathbf{e}}_1$ direction, while the bottom wall moves in the opposite direction, producing a mean velocity gradient of $\dot{\gamma} = 2U_w/H$. At $t = T/2$ the direction of the walls' velocities are rotated instantaneously about $\hat{\mathbf{e}}_2$ by an angle θ, and shear continues until $t = T$. This cycle is repeated five times to obtain an average periodic cycle for stress and fabric. Note that the periodic cycle implies a change in the direction of the walls' velocities at $t = 0$ from an angle $\theta > 0$ to $\theta = 0$. To incorporate this initial condition a previous half period is also simulated from $t = -T/2$ to $t = 0$ (see the left side of Fig. 1). The period considered is $T = 1.4/\dot{\gamma}$, enough to develop a steady state for fabric and stress in each part of the cycle. The inertial number corresponds to $I = 0.00029$, lower than the quasi-static limit of 0.001. This limit was previously verified for the reversal case to produce rate independence. The angle of rotation θ of the shear-rate tensor ranges from 30° to 180°.

3 Continuum model

3.1 Previous concepts about kinematic hardening

Kinematic hardening models are commonly used in plasticity, most commonly for metals, to model specimens subjected to cyclic loading where there exist elastic and plastic deformation. These models are capable of reproducing internal stresses that emerge in cycles of stretching and compression. In metals, the internal stresses during flow are associated with two mechanisms. The first one corresponds to plastic-strain incompatibilities between crystal grains of different orientations, and between grains and non-deformable precipitate particles. The second mechanism is associated with the polar nature of dislocations, which are formed in the forward deformation and then annihilated during reversal.[48] The generation of internal stresses manifests as hardening during tension and softening during compression, a phenomenon known as *the Bauschinger effect*.[49]

It is useful to review the essential ingredients of a backstress hardening model as exemplified by the *modified Von-Mises flow rule*:[50]

$$\boldsymbol{\tau} = \mathbf{B} + \tau_Y \frac{\mathbf{D}'_p}{|\mathbf{D}'_p|}, \quad \text{when} \quad \mathbf{D}'_p \neq \mathbf{0} \tag{2}$$

where $\mathbf{B}$ is the backstress, τ_Y is the isotropic flow resistance, and $\mathbf{D}_p$ is the plastic deformation rate tensor which combines with an elastic part to provide the total deformation rate: $\mathbf{D} = \mathbf{D}_e + \mathbf{D}_p$. We use $'$ to indicate the deviatoric part. Similarly, one defines a yield condition

$$f = |\boldsymbol{\tau} - \mathbf{B}| - \tau_Y \leq 0, \tag{3}$$

such that during plastic flow $f = 0$. One generally expresses the backstress as a multiple of a kinematic state variable measuring

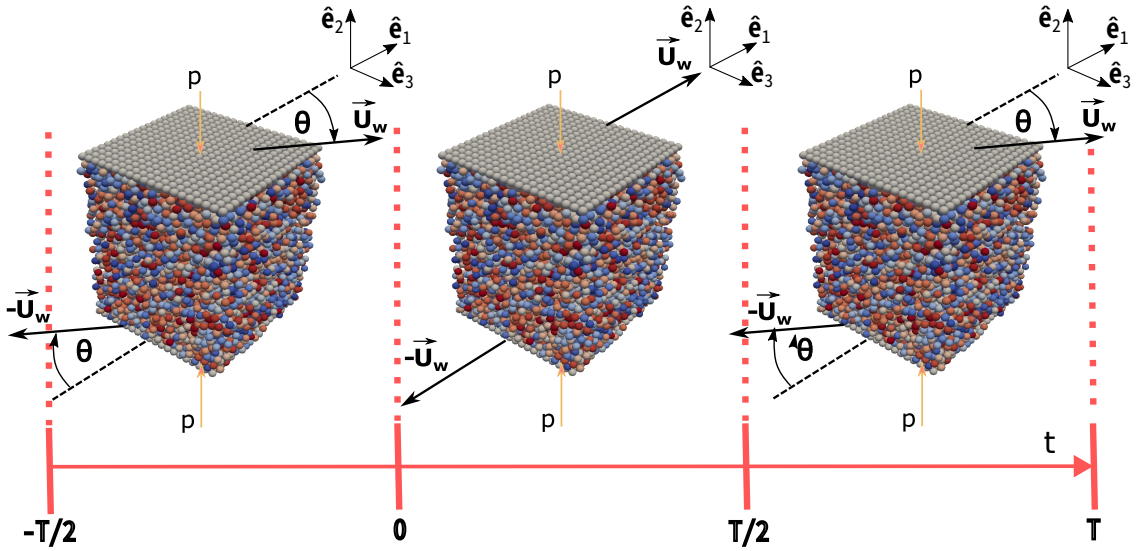

Fig. 1 Numerical setup. The red line corresponds to time, with tick marks indicating changes to the walls' velocities. The part from $t=0$ to $t=T$ corresponds to one period. A half period at the beginning was also simulated. The different walls' velocities for each part of the periodic cycle are shown. From $t=0$ to $t=T/2$, the velocity of the top wall is in the $\hat{\mathbf{e}}_1$ direction, while the bottom wall moves in the opposite direction. At $t=T/2$ the direction of the walls' velocities are rotated instantaneously by an angle θ in the plane perpendicular to $\hat{\mathbf{e}}_2$ until $t=T$. Note that there is a previous walls' rotation at $t=0$ to produce a periodic process.

internal anisotropy in the material, denoted $\mathbf{A}$, reflecting the concentration and orientation of defects:

$$\mathbf{B} \overset{\text{def}}{=} c\mathbf{A}. \tag{4}$$

The plastic flow model is then closed by positing an evolution relation for the anisotropy variable, such as

$$\overset{\triangledown}{\mathbf{A}} = k_1\mathbf{D}_p + k_2|\mathbf{D}_p|\mathbf{A}, \tag{5}$$

where $\overset{\triangledown}{\mathbf{A}} = \dot{\mathbf{A}} + \mathbf{AW} - \mathbf{WA}$ is the *Jaumann rate* of $\mathbf{A}$ with $\dot{\mathbf{A}}$ being the material time derivative of $\mathbf{A}$, and $\mathbf{W}$ the spin tensor given by $(\nabla\mathbf{v} - (\nabla\mathbf{v})^T)/2$. The Jaumann rate is a frame-indifferent tensor which is introduced to achieve objectivity in $\mathbf{A}$. In equation 5 the term $k_1\mathbf{D}_p$, where k_1 is a scalar function, grows $\mathbf{A}$ directly with the plastic strain-rate, while the expression $k_2|\mathbf{D}_p|\mathbf{A}$ represents a *recovery term* that limits the growth of $\mathbf{A}$ during steady shearing where $k_2 < 0$.[51]

As with the strain-rate, it is assumed that the strain admits a decomposition into elastic and plastic parts: $\mathbf{E} = \mathbf{E}_e + \mathbf{E}_p$ where $\mathbf{E}$ is the strain tensor. The Cauchy stress $\boldsymbol{\sigma}$ is then related to the elastic strain through an elasticity relation, such as the common linear isotropic relation:

$$\boldsymbol{\sigma} = 2\lambda\mathbf{E}_e + \left(\kappa - \frac{2}{3}\lambda\right)\mathrm{tr}\,(\mathbf{E}_e)\,\mathbf{I}. \tag{6}$$

In Eq. 6, $\mathbf{I}$ is the identity tensor, and λ and κ are scalars.

The system above relating stress, elastic/plastic deformation, and state variables is a simple elasto-plastic flow model with isotropic and kinematic hardening, and serves as the inspiration for the modeling form we will adopt for granular media in the next section. While the ultimate mathematical form inspires the model we will present, it is key to note that physically, our model has very different justification than in the case of metals, as can be seen through an analysis of the second law of thermodynamics.

The second law can be expressed as a guarantee of non-negative overall dissipation, i.e.

$$\boldsymbol{\sigma} : \mathbf{D} - \dot{\psi} \geq 0, \tag{7}$$

where ψ represents the (Helmholtz) free energy per unit volume and $\boldsymbol{\sigma} : \mathbf{D} \equiv \sum_{i,j} \sigma_{ij} : D_{ij}$ is the rate of work being done by the stress. In the case of plastically incompressible models of metals, the plastic part of the work rate, $\boldsymbol{\tau} : \mathbf{D}_p$, can sometimes be negative depending on the orientation of the backstress as implied by equation 2. However, the free energy ψ depends not only on the elastic strain but also on $\mathbf{A}$ because the defects in metals possess a separate internal energy. It is the balance between the plastic work rate and the rate of evolution of ψ, through its dependence on $\mathbf{A}$, that ensures the model always satisfies the second law inequality even when $\boldsymbol{\tau} : \mathbf{D}_p < 0$.[50]

In the case of granular media, the model we obtain also always satisfies the second law, but does so due to a compressibility mechanism that is distinct from that due to defect energy. This will be described in some detail in section 5.

3.2 Hardening variables and new fabric evolution equation

The model proposed in the present study also combines isotropic and kinematic hardening. In this model, the anisotropic kinematic variable $\mathbf{A}$ is the fabric tensor defined by:

$$\mathbf{A} = -\frac{1}{3}\mathbf{I} + \frac{1}{N_c}\sum_{c\in V}\mathbf{n}\otimes\mathbf{n}, \tag{8}$$

where $\mathbf{n}$ is the unit contact vector between two grains, and N_c the number of contacts c inside of the volume V. The evolution equation for the fabric tensor presented in this study is rooted in the equation proposed in Rojas *et al.*[39]:

$$\overset{\triangledown}{\mathbf{A}} = \alpha_1(X)\,\mathbf{D}' + \alpha_2(X)\,|\mathbf{D}'|\mathbf{A}, \tag{9}$$

where $\alpha_i(X)$ are coefficients, $X = \mathbf{A}:\mathbf{D}'/|\mathbf{D}'|$. Note that the present study considers processes where the elastic deformation is negligible so that $\mathbf{D}' \approx \mathbf{D}'_p$. This previous evolution equation, which covers only 2D transients processes, will be expanded and modified in the present work to 3D cases adding more physical arguments associated to the interplay between fabric and shear-rate. In Rojas *et al.*[39] it was shown that both coefficients α_i diverge when a reversal of the shear-rate tensor is imposed. However, this behaviour was not explained nor associated with a physical phenomenon. To address this issue, we now introduce a new scalar hardening variable S:

$$S \overset{\text{def}}{=} |\mathbf{A}| - \mathbf{A}:\frac{\mathbf{D}'}{|\mathbf{D}'|}. \tag{10}$$

Note that S is a modification of a previous state variable denoted X. The new variable S is associated with the capacity of the fabric network to keep grains in contact, which will be explained with the aid of Fig. 2. In this figure, the fabric and shear-rate tensors are drawn for simple shear at steady state and just after a shear-rate reversal. In simple shear at steady state, the grains form contact chains inclined 45° (blue circles in Fig. 2) to the shear plane. In this case, the shear-rate tensor corresponds to $\mathbf{D}' = 0.5\dot{\gamma}(\hat{\mathbf{e}}_1 \otimes \hat{\mathbf{e}}_2 + \hat{\mathbf{e}}_2 \otimes \hat{\mathbf{e}}_1)$, which is represented by red arrows in Fig. 2.a (note that $\dot{\gamma}$ is positive). On the other hand, the fabric tensor in this case has the form $\mathbf{A} = A_{12}(\hat{\mathbf{e}}_1 \otimes \hat{\mathbf{e}}_2 + \hat{\mathbf{e}}_2 \otimes \hat{\mathbf{e}}_1)$, where A_{12} is negative (blue arrows in Fig. 2.a). Since, at steady state, the fabric and shear-rate are antiparallel tensors pointing in opposite directions, we have the steady state relation $\mathbf{A} = -|\mathbf{A}|\mathbf{D}'/|\mathbf{D}'|$. Substituting this in Eq. 10, we have $S = 2|\mathbf{A}|$. On the other hand, just after a shear-rate reversal, $\mathbf{D}'$ changes its direction instantaneously, but $\mathbf{A}$ temporarily keeps its previous directionality because the contact network needs time (shear strain) to reorient (Fig. 2.b). Hence, at this moment $\mathbf{A} = |\mathbf{A}|\mathbf{D}'/|\mathbf{D}'|$, and $S = 0$.

The physical meaning of S can be explained upon rotating the coordinate system 45° (Fig. 2.c and 2.d). Figure 2.c shows that there is a compression-rate component aligned with the contact network at steady state. This situation is favorable for maintaining these contacts. In other words, the contact network resists change under this combination of $\mathbf{A}$ and $\mathbf{D}'$, which in turn is associated with a maximum S value equal to $2|\mathbf{A}|$. Figure 2.d shows the opposite situation just after the reversal, where the strain-rate acts to separate the grains without resistance. This happens because there are no attractive forces between grains to resist the stretching motion and is coincident with a zero value of the variable S. Another way to express the hardening variable S is

$$S = |\mathbf{A}|(1 - \cos(\theta_{AD})), \tag{11}$$

where $\cos(\theta_{AD}) \equiv \mathbf{A}:\mathbf{D}'/(|\mathbf{A}||\mathbf{D}'|)$. At steady state $\theta_{AD} = 180°$ and $S = 2|\mathbf{A}|$. Just after an instantaneous shear-rate reversal $\theta_{AB} = 0$ and $S = 0$. In summary, the variable S is maximal when $\mathbf{D}'$ reinforces the contacts by pushing particles together and takes a zero value (minimum value), when $\mathbf{D}'$ pulls particles apart along the contact axis.

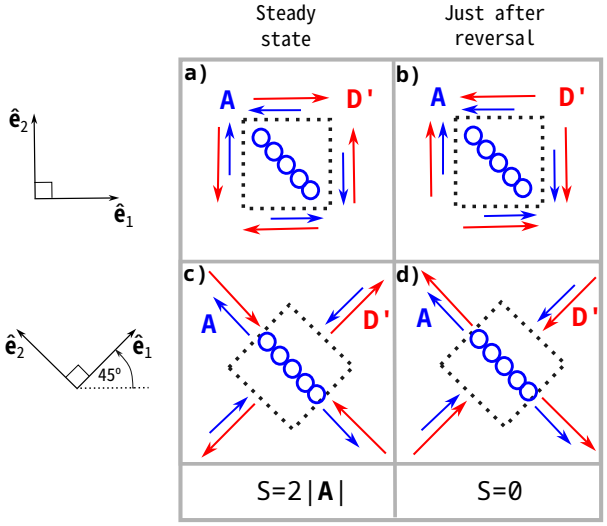

Fig. 2 Tensors' components for $\mathbf{A}$ and $\mathbf{D}'$ and S values are displayed at steady state and just after reversal for 2D simple shear. The components are showed respect to a coordinate system pointing in the horizontal and vertical direction, and respect to a second coordinated system rotated 45°.

By using equation 9, the coefficients α_i were obtained in Rojas et al.[39] from 2D DEM data collected from shear-rate reversal tests. This method was revisited for the 3D setup presented in Fig. 1, which reveals that the fabric evolution coefficients can actually be written more clearly in terms of S:

$$\alpha_i(S) = \frac{\beta_i(S)}{\Lambda(S)}. \tag{12}$$

Here, $\beta_i(S) = a_i + b_i S$ and $\Lambda(S) = S^{3/4}$. Figures 3.a and 3.b show the fit functions $\alpha_i(S)$. The factor $1/S^{3/4}$ is introduced to fit the coefficients in the diverging zone when S is near zero after reversal, while the $\beta_i(S)$ are an important part of the fit for adjusting the low slope zone to correctly approach the fabric steady state. The exponent 3/4 was obtained from the insets of figures 3.a and 3.b. Figures 3.c and 3.d show that the coefficients β_i do not diverge. The fitting parameters for β_i are shown in table 2.

The term Λ can pass to the left side in equation 9 to obtain the fabric evolution equation proposed in the present study:

$$\Lambda(S)\overset{\triangledown}{\mathbf{A}} = \beta_1(S)\,\mathbf{D}' + \beta_2(S)\,|\mathbf{D}'|\mathbf{A}. \tag{13}$$

We call the factor Λ the *contact persistence* since, as can be seen in Eq. 13, a larger Λ associates with a smaller propensity for the contact structure to change, which agrees with the previous physical analysis associated with figure 2.

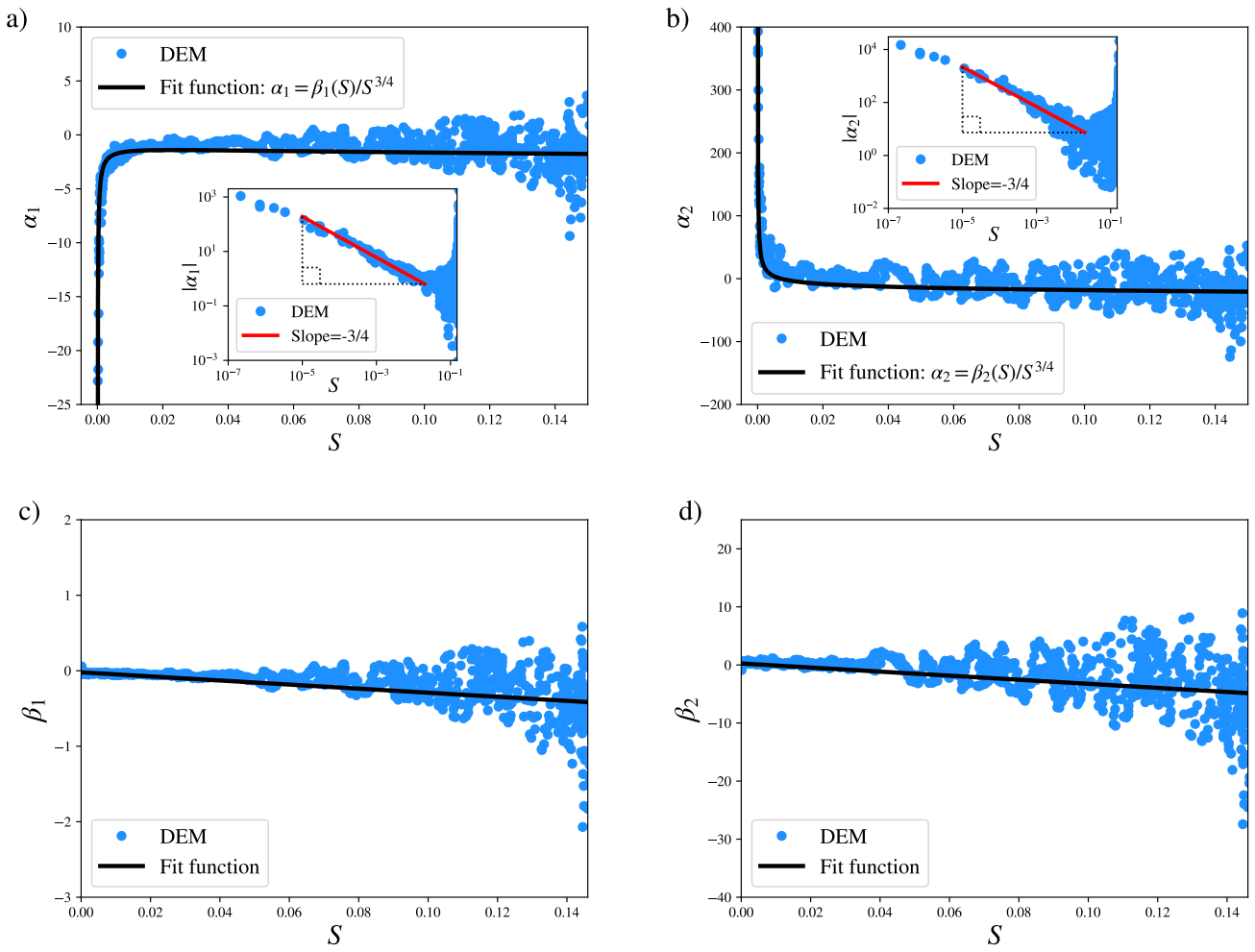

Fig. 3 Light blue points in figures a) and b) correspond to the value of the α_i coefficients from Eq. 9 versus the S hardening variable obtained from a DEM reversal (insets show the absolute values of α_i on a logarithmic scale). Fit functions $\alpha_i(S)$ are shown with solid lines. Light blue points in figures c) and d) corresponds to the β_i coefficients from equation 13 versus the S hardening variable from the DEM reversal while solid black lines represent linear fits.

3.3 Shear stress model

Unlike in Rojas et al., we now consider a shear strength model with a kinematic hardening form, using a backstress and an isotropic term. Both terms are considered proportional to the pressure like in Nemat-Nasser *et al.*[43] The backstress is assumed to be a negative multiple of the fabric tensor defined in equation (8), while the isotropic part is chosen as a multiple of the deviatoric shear-rate tensor:

$$\frac{\boldsymbol{\tau}}{p} = C(S)\mathbf{A} + Y(S)\frac{\mathbf{D}'}{|\mathbf{D}'|}, \quad \text{when} \quad \mathbf{D}' \neq \mathbf{0}. \tag{14}$$

The functions $C(S)$ and $Y(S)$ were obtained from DEM simulations rotating the walls' velocities, as per Fig. 1, from $\theta = 30°$ to $170°$. For this purpose, at each instant, C and Y were considered as unknowns in equation 14 and solved using the off-diagonal components of this equation. Note that it is not possible to calibrate C and Y using reversal data only ($\theta = 180°$), since equation 14 only has one component in this case. This may explain why studies based on 2D DEM data have not discovered the underlying backstress model. Figure 4 shows the DEM results for C and Y and the fit functions for the shear stress model.

Figure 4.a shows that C obtained from DEM simulations is always close to a constant value, which corresponds to $C = -5.6$. The DEM results for Y are well-approximated by the linear function $Y = n + mS$ (see Fig. 4.b). Table 1 shows a summary of all the equations in the flow model proposed, and Table 2 shows the fitted values of the parameters.

4 Results

We solve the continuum model proposed in the present work using an explicit numerical method for equation 13 to obtain the evolution of the fabric tensor. Then the stress is obtained using equation 14. Since the problem is periodic in time, the initial conditions for equation 13 are the final fabric tensor values of each period of time, which we take from the same model results. Figures 5 and 6 show the evolution of the off-diagonal components for fabric and stress during transients compared with DEM simulations. Six θ angles for the shear-rate rotation were eval-

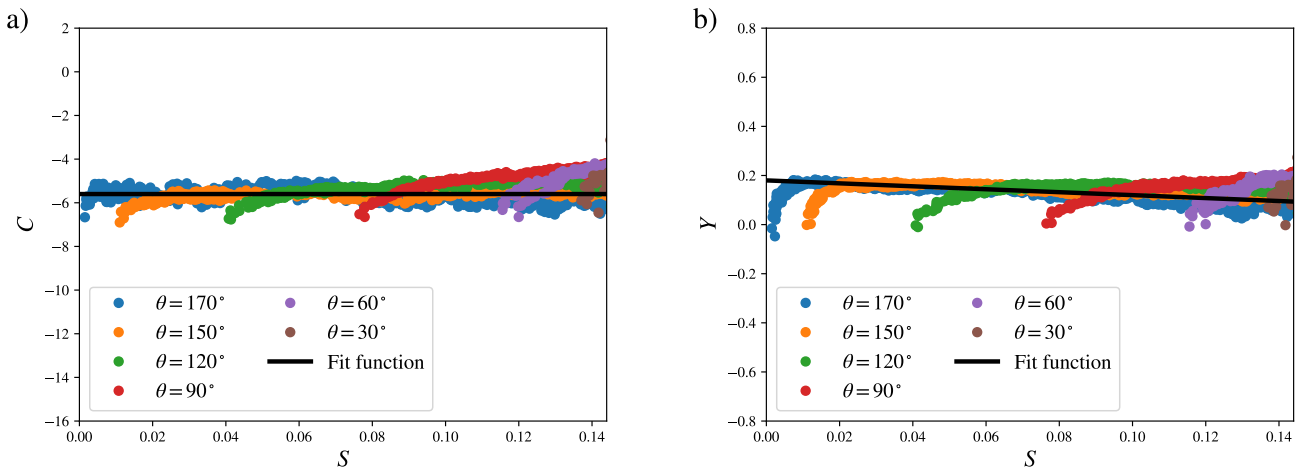

Fig. 4 DEM results and fit functions for the shear stress model proposed in the present work (Eq. 14). a) Backstress parameter C, b) Yield function $Y(S)$.

Rule or relation	Equation	Number
Flow rule	$\frac{\boldsymbol{\tau}}{p} = C\mathbf{A} + Y(S)\frac{\mathbf{D}'}{\lvert\mathbf{D}'\rvert}$	(20)
Scalar hardening variable	$S = \lvert\mathbf{A}\rvert - \mathbf{A} : \frac{\mathbf{D}'}{\lvert\mathbf{D}'\rvert}$	(21)
Yield function	$Y(S) = n + mS$	(22)
Fabric evolution equation	$\Lambda(S)\overset{\nabla}{\mathbf{A}} = \beta_1(S)\mathbf{D}' + \beta_2(S)\lvert\mathbf{D}'\rvert\mathbf{A}$	(23)
Contact persistence	$\Lambda(S) = S^{3/4}$	(24)
Fabric equation coefficients	$\beta_i(S) = a_i + b_i S$	(25)

Table 1 Summary of the equations involved in the isotropic and kinematic hardening model described in sections 3.2 and 3.3.

Fitting parameters
Backstress constant
$C = -5.6$
Yield function parameters
$n = 0.18$
$m = -0.60$
Fabric equation parameters
$a_1 = -0.021$
$b_1 = -2.7$
$a_2 = 0.25$
$b_2 = -35$

Table 2 Summary of the calibration parameters involved in the isotropic and kinematic hardening model presented in Table 1.

uated ($30°, 60°, 90°, 120°, 150°$, and $180°$). Both models for fabric and stress are in agreement with the DEM simulations for all the cases analyzed. This agreement is stronger for angles between $30°$ and $90°$, and also for the reversal case ($\theta = 180°$), while for $120°$ and $150°$ the model presents a faster arrival to the steady state for the smaller fabric and stress components.

A specific case of interest is $\theta = 90°$ (Figs. 5.e and 5.f), where the first half of the cycle is only in the plane perpendicular to $\hat{\mathbf{e}}_3$ (D_{12} component), while the second half is only in the plane $\hat{\mathbf{e}}_1$ (D_{32} component). Here, the stress is always in a rate-independent relaxation process in a plane where there is no shear strain-rate. For example, the τ_{32} component is relaxing from its steady state value to zero during the first part of the period (see blue points in Fig. 5.f). The values of τ_{32} remain non-zero for almost the entire first half of the cycle even though D_{32} is zero. During this time the shear stress and shear-rate tensors are highly misaligned. The stress relaxation corresponds to a backstress evolution in the plane without shearing and produces stress components that are well-matched by the new model, equation 14 (black curves in Fig. 5.f). In contrast, the vast majority of existing granular flow models presume alignment of the principal directions of shear-rate and shear stress, which would incorrectly give $\tau_{32} = 0$ for the entire first half of the cycle. An identical backstress relaxation occurs for τ_{12} during the second half of the period, which is also well predicted by the new stress model.

The model presented in this study was also tested applying shear-rate rotation while transient relaxations are still in process to verify its robustness. Figure 7 shows the results of the rotation for $\theta = 90°$ at the intermediate dimensionless times: $t\dot{\gamma} = 0.1$ and $t\dot{\gamma} = 0.2$. The model shows a good agreement with DEM simulations for all the fabric and stress off-diagonal components.

The shear stress can be also analyzed by comparing the two parts that make it up: the backstress from $\mathbf{B}$ and the isotropic part whose magnitude is Y. Figure 8.a shows a comparison of these two parts in the shear-rate reversal case. The first observation is the large magnitude of the backstress, which corresponds to 88% of the shear stress at steady state. A second observation is that the isotropic stress is greater near $S = 0$, which is well-captured by the

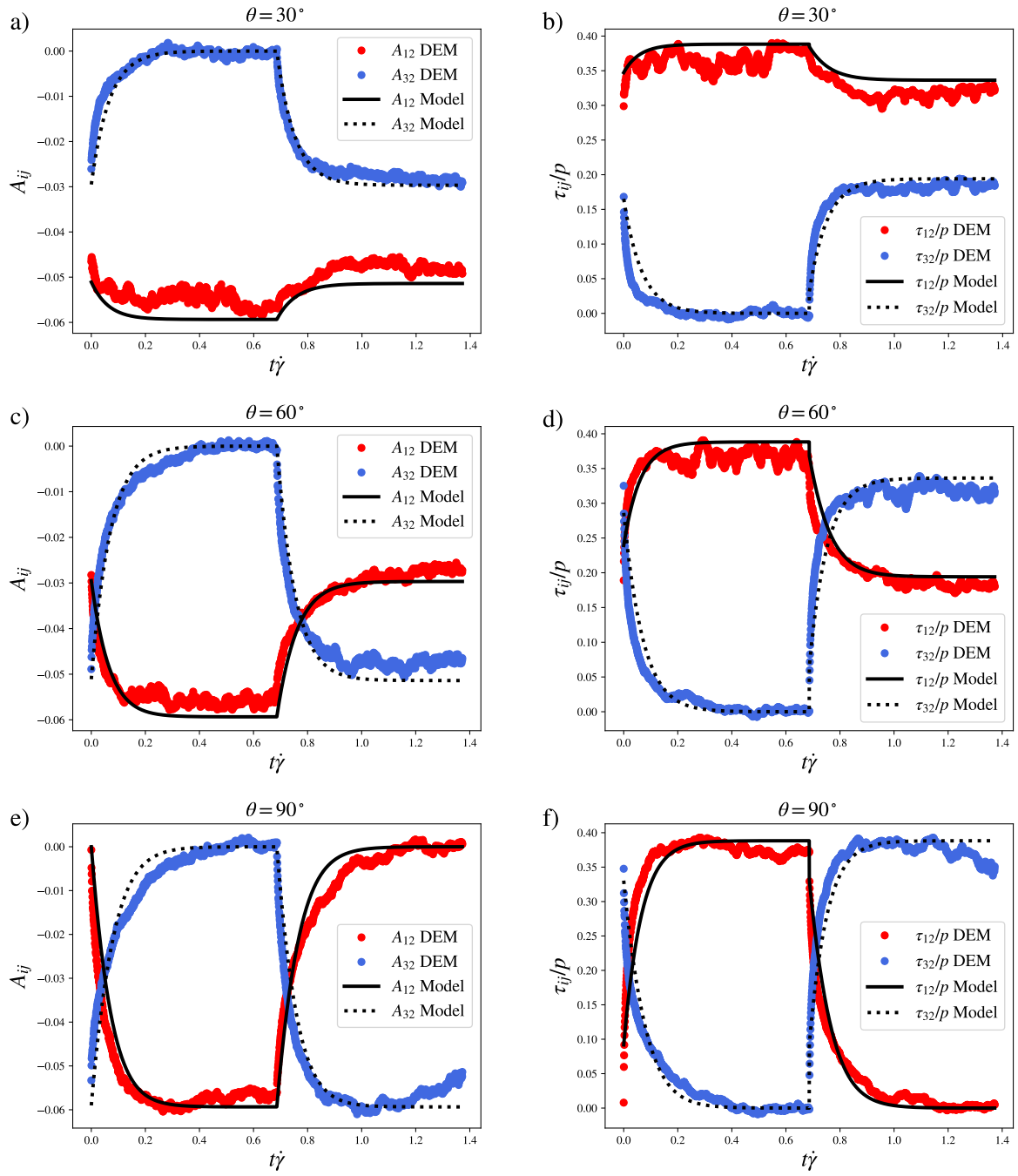

Fig. 5 Comparison between model and DEM simulations of the off-diagonal components of the fabric and normalized shear stress during transients. The angles θ of the shear-rate rotation corresponds to $[30°, 60°, 90°]$. Figures a), c), and e): fabric components comparison. Figures b), d), and f): comparison of the normalized shear stress components.

model due to the negative slope of the yield function $Y = Y(S)$. A last observation arises by comparing the relaxation times of both terms. Following the DEM data in figure 8.a, the isotropic part approaches steady state at $t\dot{\gamma} = 0.25$, while the backstress has a slower relaxation of $t\dot{\gamma} = 0.6$, which is more than double.

This last observation, combined with the presumption that C is a constant, allows us to calibrate the new shear stress model using only a reversal DEM test. When the shear stress is nearing steady state after a reversal, only the backstress is still evolving, and thus $\Delta\tau_{12} \approx \Delta B_{12} = C\Delta A_{12}$. Therefore, near the steady state after a shear-rate reversal, it is possible to compute C as

$$C \approx \frac{\Delta\tau_{12}}{\Delta A_{12}}, \tag{15}$$

as shown in figure 8.b. This linear slope near the steady state when τ_{12} is plotted versus A_{12} after a reversal is also present in other studies.[38,39] The yield function Y can be obtained from the

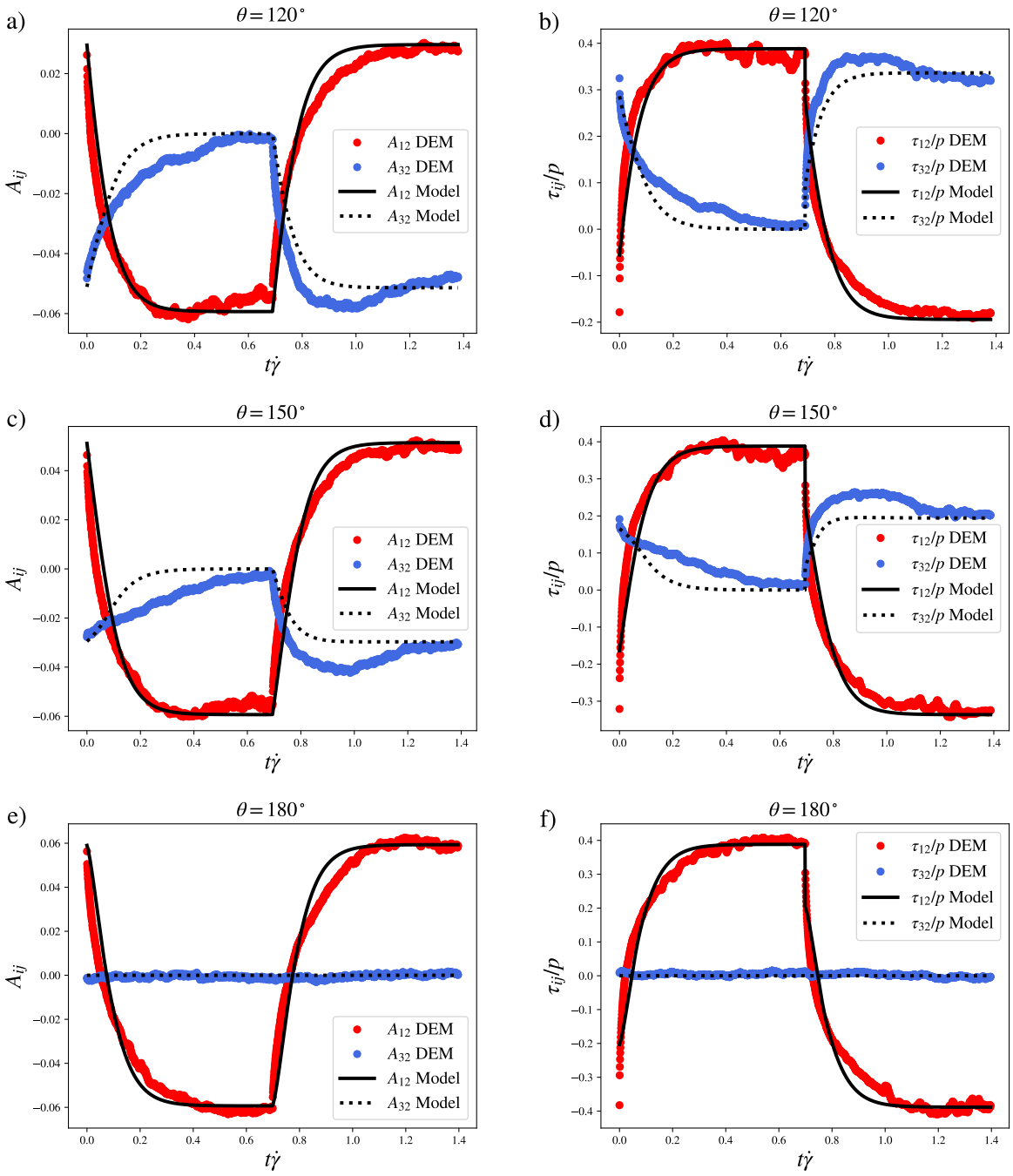

Fig. 6 Comparison between model and DEM simulations of the off-diagonal components of the fabric and normalized shear stress during transients. The angles θ of the shear-rate rotation corresponds to $[120^\circ, 150^\circ, 180^\circ]$. Figures a), c), and e): fabric components comparison. Figures b), d), and f): comparison of the normalized shear stress components.

same reversal DEM data by plotting

$$Y = \left(\frac{\boldsymbol{\tau}}{p} - C\mathbf{A}\right) : \frac{\mathbf{D}'}{|\mathbf{D}'|}, \tag{16}$$

as a function of the scalar hardening variable S. Finally, the fabric evolution can be calibrated by using the same procedure from before, which is based on considering β_i as unknowns in Eq. 13.

5 Second-law justification of model

The justification for a backstress appearing in kinematically hardening metals is that the free energy function has a defect energy contribution, which evolves in such a way to cancel any negative plastic work-rate that may occur due to the backstress. In a granular material it is not clear that the free energy should have a separate contribution depending only on $\mathbf{A}$. Microscopically, such a defect energy would require a way for grains to remain compressed (i.e. store energy) even when all external confining

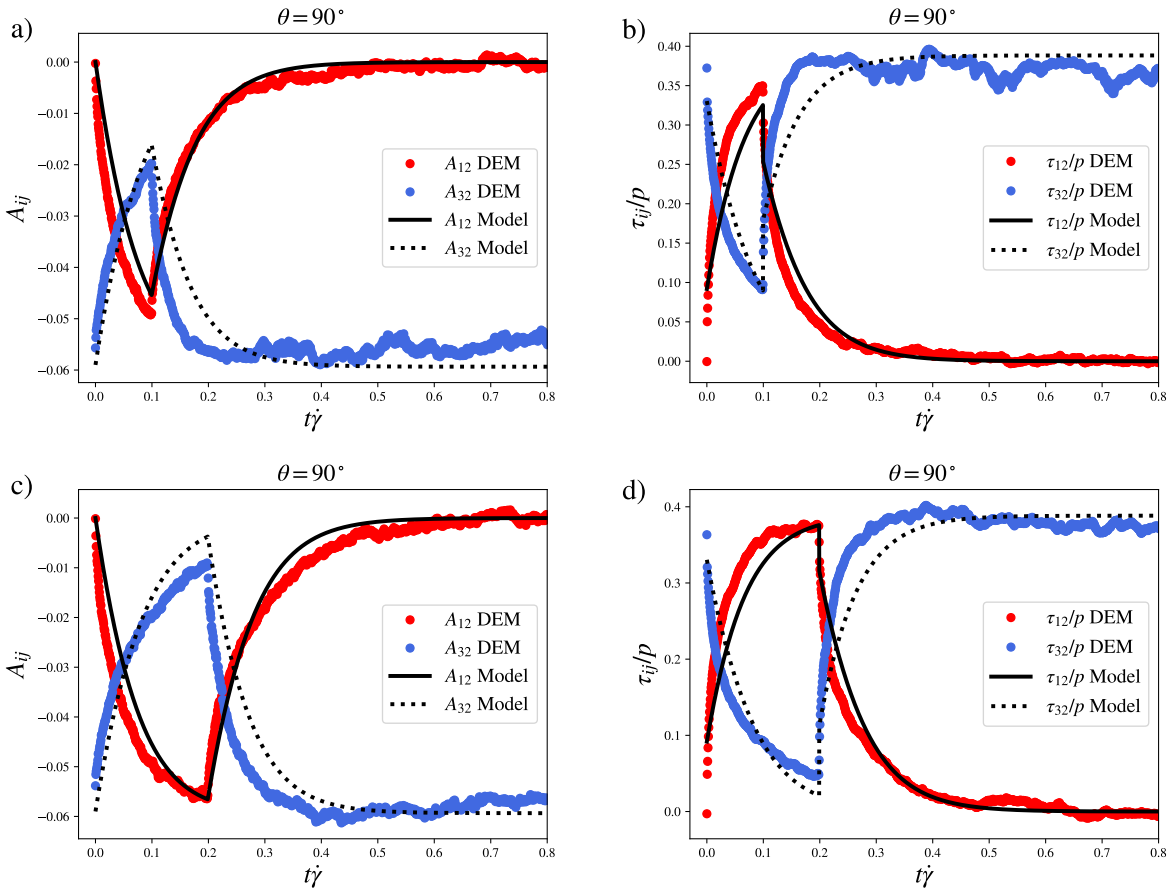

Fig. 7 Comparison between model and DEM simulations of the off-diagonal components of the fabric and normalized shear stress during transients for $\theta = 90^\circ$ rotated at small strains. Figures a) and b) show the fabric and normalized shear stress components for a change in the shear orientation at $t\dot{\gamma} = 0.1$, while for figures c) and d) the change is when $t\dot{\gamma} = 0.2$.

stresses are removed, which would be seemingly impossible for cohesionless grains. That said, the flow model we have presented still admits the possibility that $\boldsymbol{\tau} : \mathbf{D}'$ is negative, which typically occurs just after reversal when $\boldsymbol{\tau}$ has the opposite direction as $\mathbf{D}'$ due to the fabric (and hence backstress) needing time to change from the state before reversal. One might ask, how does such a model not violate the second law?

The key to understanding this point is to realize that shearing a granular material under constant pressure does not produce isochoric motion, but rather produces a noticeable dilation/contraction that evolves during flow. Suppose for ease of derivation that the elastic moduli of the grain material are high enough that the elastic work-rate and elastic strain are always small, such that all motion can be viewed as purely plastic motion. Then $\mathbf{D} \approx \mathbf{D}_p$, $\psi = \dot{\psi} = 0$, and we can write the second law as

$$0 \leq \boldsymbol{\sigma} : \mathbf{D} = \boldsymbol{\tau} : \mathbf{D}' - p\,\mathrm{tr}\mathbf{D} = \boldsymbol{\tau} : \mathbf{D}' + p\dot{\Phi}/\Phi, \tag{17}$$

where Φ is the packing fraction. It is important to note that if dilation is non-zero, the $p\dot{\Phi}/\Phi$ term is nonzero and has the potential to compensate for any negative work-rate from $\boldsymbol{\tau} : \mathbf{D}'$. An analysis of DEM data in figure 9(a) confirms that even though $\boldsymbol{\tau} : \mathbf{D}'$ can be negative immediately after flow reversal, the high compaction-rate that occurs then causes an even larger, positive $p\dot{\Phi}/\Phi$ contribution, which compensates to produce an overall plastic work-rate that is always non-negative*. Thus, the second law is always satisfied in these flows in spite of the occasional negativity of the shear work-rate with no need to appeal to a defect energy.

Since the fabric/flow model we have presented focuses solely on shearing behavior, we should be able to show that, when coupled to an appropriate dilation model, the model in its entirety is mathematically incapable of violating the second law. Thus, we present and briefly validate a simple dilation model below.

Two basic assumptions can be used to guide the modeling of granular dilatancy: (1) the packing fraction increases just after flow reversal when $\mathbf{A} : \mathbf{D}' > 0$, since contacts are being separated and the structure is collapsing, and (2) in steady forward shearing the packing fraction should evolve toward a constant critical state value Φ_c. A simple rule obeying these assumptions is:

$$\dot{\Phi}/\Phi = c_1 \mathbf{A} : \mathbf{D}' + c_2 \left(\Phi_c - \Phi + c_3\right)|\mathbf{D}'| \tag{18}$$

for positive scalars c_1, c_2, c_3. The first term drives the packing

* A few data points appear to produce negative overall work just after the reversal, but this is actually from the very small elastic unloading of the grains, which should be excluded since its motion is not part of $\mathbf{D}_p$

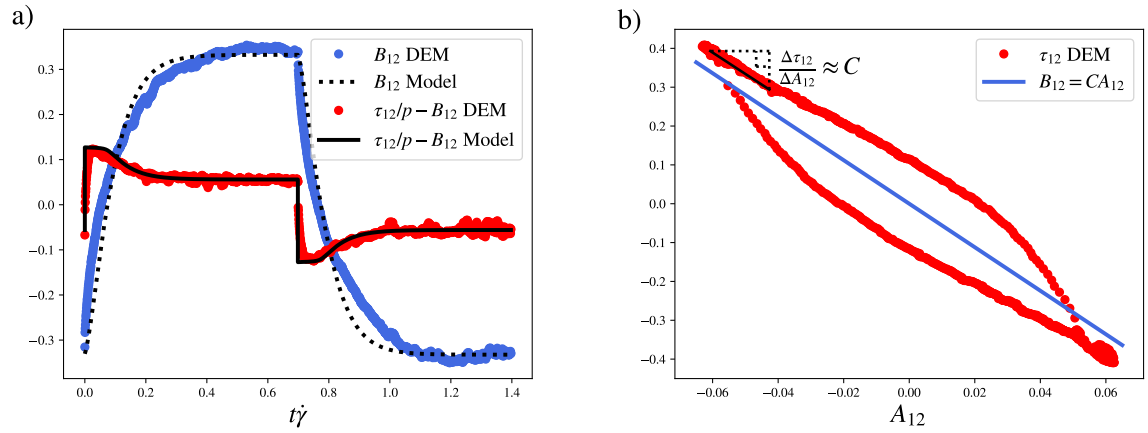

Fig. 8 Analysis of the stress evolution during the reversal case. a) Backstress and isotropic flow resistance. b) Shear stress component τ_{12} versus fabric component A_{12}.

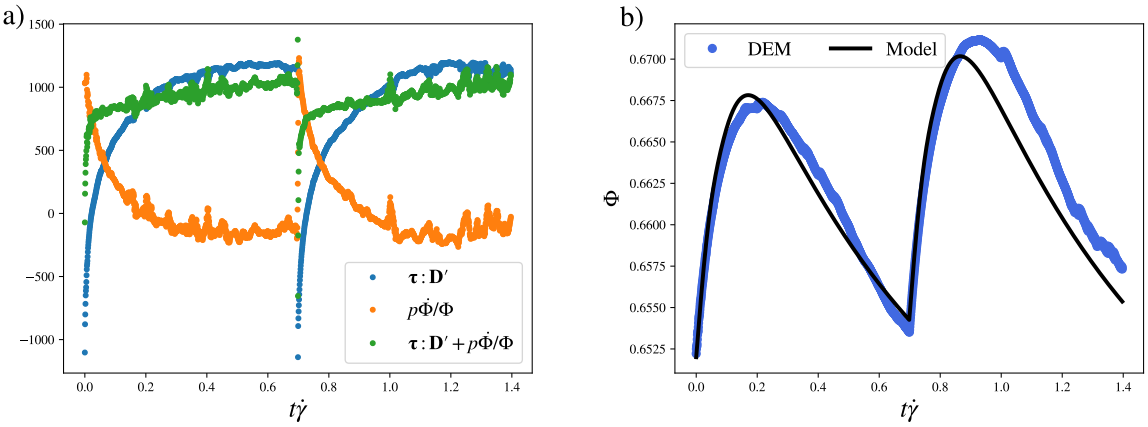

Fig. 9 (a) DEM data comparing the work-rate due to shear (blue), the work-rate due to volume change (orange), and the total work-rate $\boldsymbol{\sigma}:\mathbf{D} = \boldsymbol{\tau}:\mathbf{D}' + p\dot{\Phi}/\Phi$ (green) over a forward-reversal cycle in the $\theta = 180^\circ$ case. (b) The packing fraction over the same time range obtained in DEM and from the dilation model, equation 18.

fraction to rise with shear when $\mathbf{A}:\mathbf{D}'$ is positive, which occurs just after reversal. The quantity c_2c_3 must be chosen to approach the steady state value of $-c_1\mathbf{A}:\mathbf{D}'/|\mathbf{D}'|$ so that Φ evolves toward a constant critical state value of Φ_c in steady shearing. This model bears a number of similarities to models previously presented for dilation[38].

Substituting this dilation relation and equation 14 into the total work rate, we obtain

$$\begin{aligned}\boldsymbol{\sigma}:\mathbf{D} &= \boldsymbol{\tau}:\mathbf{D}' + p\dot{\Phi}/\Phi \\ &= p\left(C\mathbf{A} + Y\mathbf{D}'/|\mathbf{D}'|\right):\mathbf{D}' + p\left(c_1\mathbf{A}:\mathbf{D}' + c_2\left(\Phi_c - \Phi + c_3\right)|\mathbf{D}'|\right) \\ &= p\left(Y|\mathbf{D}'| + (C+c_1)\mathbf{A}:\mathbf{D}' + c_2\left(\Phi_c - \Phi + c_3\right)|\mathbf{D}'|\right).\end{aligned}$$

Since $Y, p, c_1, c_2, c_3 \geq 0$, the work rate formula above is necessarily ≥ 0, for any $\mathbf{A}$ and $\mathbf{D}'$, if the parameters are chosen to satisfy

$$c_1 = -C \text{ and } \Phi \leq \Phi_c + c_3\,. \tag{19}$$

Figure 9(b) shows the packing fraction evolution in DEM versus the results of the dilation model for $c_1 = -C = 5.6$, $c_2 = 5.6S^{1/3}$, $c_3 = 0.14$, and $\Phi_c = 0.652$. It can be seen that the model compares favorably to DEM with these values, which satisfy the constraints in equation 19, with c_2c_3 approaching $-c_1\mathbf{A}:\mathbf{D}'/|\mathbf{D}'|$ as required.

We have thus shown that a simple dilation model can be found that agrees with DEM data, captures the essential ingredients of transient granular dilatancy, and guarantees the model for shear flow is justified thermodynamically under the second law. To be clear, it is not the primary intention of this paper to present a dilatancy model. We present it simply to validate the physical grounds of the fabric/shear-flow model we have introduced. Doing so also shows how a relation between volume change and fabric structure can give rise to a justifiable backstress in the shear strength, offering an alternative route to the typical explanation for backstresses based on defect energy in metal plasticity.

Conclusions and final remarks

The present work presents a three-dimensional granular flow model for predicting the fabric and shear stress history when the medium is subjected to cycles of unaligned shearing. The model,

based on combined isotropic and kinematic hardening, considers a fabric evolution equation and a flow rule. The fabric tensor evolution is a differential equation built under three tenets proposed in this work: 1) there is an *input term*, proportional to the shear-rate tensor, that can act to modify the contact structure of a granular assembly; 2) the medium balances the input by means of a *recovery term*, proportional to the fabric; and 3) there exists a *contact persistence* that scales the overall rate-of-change of fabric, which depends on the relative direction of the shear-rate with respect to the fabric tensor. This conceptualization allows us to pose the evolution equation as a cause-effect process, giving us a physical sense of the fabric transient response.

The flow rule for the media's shear strength, consists of: 1) a structural term or *backstress*, proportional to the fabric tensor; and 2) an *isotropic term*, proportional to the unit shear-rate tensor. This decomposition is supported by DEM data obtained through a methodology to relax the contact structure and shear stress out of the plane of shearing. By including the backstress, the model links directly the mesoscale, represented by the fabric tensor, with the shear stress. On the other hand, the isotropic part of the model resists any motion in any direction. The entire model can be calibrated by using only a reversal test, as we explained at the end of section 4, avoiding the necessity to perform more complex 3D tests.

Through 3D DEM simulations the existence of the backstress during transient and steady state was demonstrated. Also, the backstress constitutes the largest part of the shear stress resistance in simple shear, which is consistent with the idea of the connection between the structure of the granular medium and its resistance to flow. There is a good agreement between the results of the model and DEM simulations over off-diagonal components of the fabric and shear stress, when a sudden shear-rate rotation is imposed to the granular system. Note that this comparison was made for almost the entire possible range of the rotation of shear direction (between 30° and 180°).

Backstress-based models were developed in metal plasticity and their effectiveness here draws an interesting connection between these materials. However, in metals they are justified by introducing a free-energy contribution due to microscopic anisotropic internal defects, whose stored energy remains even when macroscopic stresses on the system are released. On the other hand, we have shown that the backstress in granular media is of a different physical origin even if it ultimately produces a transient shear-flow model with many of the same mathematical features. In granular flow, the backstress does not arise from energetic effects but rather because the packing fraction evolution is influenced directly by the fabric tensor, with densification occurring when the fabric and flow-rate tensors align. There are in fact two parallel phenomena that occur just after a shear-rate reversal. First, in the stretching direction aligned with the contact network, grains are separated with no resistance, which is consistent with a null contact persistence. At the same time, in the perpendicular direction, the grains are pushed closer at an angle where the contact structure is not yet present to resist this movement, inevitably producing a compression of the granular medium.

Finally, the model proposed in this work was tested only in the quasi-static regime, and always considering shearing. More rapid, inertial cases should be analyzed to find coefficients as a function of the inertial number for the fabric evolution equation and flow rule. Compression-stretching displacements could be analyzed in the future to model the fabric and stress diagonal components. The existence of backstress in other granular materials, like those comprised of elongated particles, could also be tested.

Conflicts of interest

There are no conflicts to declare.

Data availability

A Python script to run the model presented previously in comparison with the DEM data used in this article is available at DOI: `https://doi.org/10.6084/m9.figshare.28447418.v1`

Acknowledgements

The authors thank Agencia Nacional de Investigación y Desarrollo (ANID-Chile) for financially supporting this research through Fondecyt Grant: 11230970 (E.R.).

References

1 G. M. gdrmidi@ polytech. univ-mrs. fr http://www. lmgc. univ-montp2. fr/MIDI/, *The European Physical Journal E*, 2004, **14**, 341–365.

2 F. Da Cruz, S. Emam, M. Prochnow, J.-N. Roux and F. Chevoir, *Physical Review E-Statistical, Nonlinear, and Soft Matter Physics*, 2005, **72**, 021309.

3 O. Pouliquen, C. Cassar, P. Jop, Y. Forterre and M. Nicolas, *Journal of Statistical Mechanics: Theory and Experiment*, 2006, **2006**, P07020.

4 P. Jop, Y. Forterre and O. Pouliquen, *Nature*, 2006, **441**, 727–730.

5 P. Jop, *Physical Review E–Statistical, Nonlinear, and Soft Matter Physics*, 2008, **77**, 032301.

6 L. Staron, P. Y. Lagrée and S. Popinet, *The European Physical Journal E*, 2014, **37**, 1–12.

7 K. Kamrin, *Frontiers in Physics*, 2019, **7**, 116.

8 K. Kamrin, K. M. Hill, D. I. Goldman and J. E. Andrade, *Annual Review of Fluid Mechanics*, 2024, **56**, 215–240.

9 K. Kamrin and G. Koval, *Physical review letters*, 2012, **108**, 178301.

10 D. L. Henann and K. Kamrin, *Proceedings of the National Academy of Sciences*, 2013, **110**, 6730–6735.

11 K. Kamrin and D. L. Henann, *Soft matter*, 2015, **11**, 179–185.

12 M. Bouzid, M. Trulsson, P. Claudin, E. Clément and B. Andreotti, *Physical review letters*, 2013, **111**, 238301.

13 M. Bouzid, A. Izzet, M. Trulsson, E. Clément, P. Claudin and B. Andreotti, *The European Physical Journal E*, 2015, **38**, 1–15.

14 A. Drescher and G. D. J. De Jong, *Journal of the Mechanics and Physics of Solids*, 1972, 337–340.

15 P. A. Cundall and O. D. Strack, *geotechnique*, 1979, **29**, 47–65.

16 B. Utter and R. Behringer, *The European Physical Journal E*, 2004, **14**, 373–380.

17 E. Rojas, M. Trulsson, B. Andreotti, E. Clément and R. Soto, *Europhysics Letters*, 2015, **109**, 64002.

18 L. Lacaze and R. R. Kerswell, *Physical Review Letters*, 2009, **102**, 108305.

19 P.-Y. Lagrée, L. Staron and S. Popinet, *Journal of Fluid Mechanics*, 2011, **686**, 378–408.

20 S. Dunatunga and K. Kamrin, *Journal of Fluid Mechanics*, 2015, **779**, 483–513.

21 A. Franci and M. Cremonesi, *Journal of Computational Physics*, 2019, **378**, 257–277.

22 A. Salehizadeh and A. Shafiei, *Granular Matter*, 2019, **21**, 32.

23 R. Valette, S. Riber, L. Sardo, R. Castellani, F. Costes, N. Vriend and E. Hachem, *Computers & Fluids*, 2019, **191**, 104260.

24 C.-C. Lin and F.-L. Yang, *Journal of Computational Physics*, 2020, **420**, 109708.

25 C. Juez, D. Caviedes-Voullième, J. Murillo and P. García-Navarro, *Computers & Geosciences*, 2014, **73**, 142–163.

26 J. M. N. T. Gray, *Dynamic Response of Granular and Porous Materials under Large and Catastrophic Deformations*, 2003, 3–42.

27 Y. Forterre and O. Pouliquen, *Journal of Fluid Mechanics*, 2003, **486**, 21–50.

28 A. Babeyko and S. V. Sobolev, *Lithos*, 2008, **103**, 205–216.

29 A. N. Schofield and P. Wroth, *Critical state soil mechanics*, McGraw-hill London, 1968, vol. 310.

30 N. Khalili, M. Habte and S. Valliappan, *International journal for numerical methods in engineering*, 2005, **63**, 1939–1960.

31 A. Golchin and A. Lashkari, *International Journal of Solids and Structures*, 2014, **51**, 2807–2825.

32 Z.-Y. Yin, Q. Xu and P.-Y. Hicher, *Acta Geotechnica*, 2013, **8**, 509–523.

33 I. Einav, *International Journal of Solids and Structures*, 2012, **49**, 1305–1315.

34 S. Larsson, J. M. Rodríguez Prieto, G. Gustafsson, H.-Å. Häggblad and P. Jonsén, *Computational Particle Mechanics*, 2021, **8**, 135–155.

35 E. DeGiuli, J. McElwaine and M. Wyart, *Physical Review E*, 2016, **94**, 012904.

36 V. Magnanimo and S. Luding, *Granular Matter*, 2011, **13**, 225–232.

37 N. Kumar, O. I. Imole, V. Magnanimo and S. Luding, *Particuology*, 2014, **12**, 64–79.

38 J. Sun and S. Sundaresan, *Journal of Fluid Mechanics*, 2011, **682**, 590–616.

39 E. Rojas Parra and K. Kamrin, *Granular Matter*, 2019, **21**, 1–7.

40 R. S. Rivlin, *Collected Papers of RS Rivlin: Volume I and II*, Springer, 1955, pp. 1014–1035.

41 P. Fu and Y. F. Dafalias, *International Journal for numerical and analytical methods in geomechanics*, 2011, **35**, 1918–1948.

42 M. Amereh and B. Nadler, *Journal of Fluid Mechanics*, 2022, **936**, A40.

43 S. Nemat-Nasser and J. Zhang, *International Journal of Plasticity*, 2002, **18**, 531–547.

44 P. Acharya and M. Trulsson, *Physical Review Research*, 2024, **6**, 033327.

45 F. Blanc, F. Peters, J. J. Gillissen, M. E. Cates, S. Bosio, C. Benarroche and R. Mari, *Physical Review Letters*, 2023, **130**, 118202.

46 R. Seto, A. Singh, B. Chakraborty, M. M. Denn and J. F. Morris, *Granular Matter*, 2019, **21**, 1–8.

47 V. Šmilauer, B. Chareyre, J. Duriez, A. Eulitz, A. Gladky, N. Guo, C. Jakob, J. Kozicki, F. Kneib, C. Modenese *et al.*, *Yade documentation*, 2015, **10**,.

48 L. Anand and S. Govindjee, *Continuum mechanics of solids*, Oxford University Press, 2020.

49 J. Lemaitre and J.-L. Chaboche, *Mechanics of solid materials*, Cambridge university press, 1994.

50 M. E. Gurtin, E. Fried and L. Anand, *The mechanics and thermodynamics of continua*, Cambridge university press, 2010.

51 P. J. Armstrong, C. O. Frederick *et al.*, *A mathematical representation of the multiaxial Bauschinger effect*, Berkeley Nuclear Laboratories Berkeley, CA, 1966, vol. 731.

A Python script to run the model presented previously in comparison with the DEM data used in this article is available at DOI:

https://doi.org/10.6084/m9.figshare.28447418.v1